

# Soft Matter

Accepted Manuscript



This is an *Accepted Manuscript*, which has been through the Royal Society of Chemistry peer review process and has been accepted for publication.

*Accepted Manuscripts* are published online shortly after acceptance, before technical editing, formatting and proof reading. Using this free service, authors can make their results available to the community, in citable form, before we publish the edited article. We will replace this *Accepted Manuscript* with the edited and formatted *Advance Article* as soon as it is available.

You can find more information about *Accepted Manuscripts* in the [Information for Authors](#).

Please note that technical editing may introduce minor changes to the text and/or graphics, which may alter content. The journal's standard [Terms & Conditions](#) and the [Ethical guidelines](#) still apply. In no event shall the Royal Society of Chemistry be held responsible for any errors or omissions in this *Accepted Manuscript* or any consequences arising from the use of any information it contains.



## Soft Matter

## PAPER

# Molecular Assembly of Highly Symmetric Molecules under Hydrogen Bond Framework Controlled by Alkyl Building Blocks: A Simple Approach to Fine-tune Nanoscale Structures

Received 00th January 20xx,  
Accepted 00th January 20xx

DOI: 10.1039/x0xx00000x

www.rsc.org/

Pimsai Tanphibul,<sup>a</sup> Kohji Tashiro<sup>\*,b</sup> and Suwabun Chirachanchai<sup>\*,a,c</sup>

Up to the present, molecular assemblies under the contribution of hydrogen bond in combination with weak interactions and their consequent morphologies have been variously reported; however, how the systematic variation of the structure can fine-tune the morphologies has not yet been answered. The present work finds the answer through highly symmetric molecules, i.e. diamine-based benzoxazine dimers. This type of molecule develops unique molecular assemblies with their networks formed by the hydrogen bond at the terminal, while, at the same time, the hydrogen bonded frameworks are further controlled by the hydrophobic segment at the center of the molecule. When this happens, slight differences in hydrophobic alkyl chain lengths (**C2**, **C4**, **C6** and **C8**) bring a significant change to the molecular assemblies, resulting in tunable morphologies, i.e. spheres, needles and dendrites. The superimposition between the crystal lattice obtained from X-ray single crystal analysis and the electron diffraction pattern obtained from the transmission electron microscope allows us to identify the molecular alignment from single molecules to self-assembly until morphologies developed. The present work, for the first time, shows the case of symmetric molecules that the hydrophobic building block controls in hydrogen bond patterns, leading to the variation of molecular assemblies with tunable morphologies.

## 1 Introduction

The understanding of supramolecular architectures of self-assemblies is an essential prerequisite to develop nanoscale materials with specific properties.<sup>1-4</sup> The self-assemblies organized through the noncovalent interactions, so-called weak interactions, i.e. hydrogen bond<sup>5</sup>,  $\pi$ - $\pi$  stacking<sup>6</sup>, and hydrophobic van der Waals are reported to be one of the key factors. Under those weak interactions, the self-assemblies develop the well-defined supramolecular structures and direct the nano- or microscopic morphologies<sup>7</sup> to be, for example, micelles<sup>8</sup>, vesicles<sup>9-11</sup>, tubes<sup>12</sup>, rods<sup>13</sup>, wires<sup>14-16</sup>, helices<sup>17, 18</sup>, etc.<sup>19-21</sup>

Up to the present, self-assemblies with specific morphologies under the role of hydrogen bonds have been variously reported. Great attention is now being paid to hydrogen bonds in cooperation with other weak interactions such as  $\pi$ - $\pi$  stacking and hydrophobic van der Waals since these systems can mimic the natural supramolecular structures to show definite

18 nanostructures.<sup>22-25</sup> For example, Sun *et al.* showed the self-assembly of perylene- and lysine-containing molecules that create various morphologies based on the nanostructures under hydrogen bonds with  $\pi$ - $\pi$  stacking.<sup>17</sup> Moyer *et al.* demonstrated the self-assembly of peptide amphiphile in twisting morphology due to the combination of hydrogen bonds of the peptide segment and the hydrophobic-hydrophobic tail in the molecule.<sup>26</sup>

Thus, the question arises as to whether the hydrogen bond can be systematically controlled by changing cooperative weak interactions among the molecules in order to direct the organization of self-assemblies and fine-tune the morphologies or not. This study considers the symmetric molecules with two hydroxyl groups at each terminal and the alkyl chains in between. The systematic variation of the alkyl chains might lead to easily visualized changes in self-assembly patterns and the consequent tunable morphologies.

Based on the above mentioned approach, mono-phenol based benzoxazine, which can be obtained from mono-phenol, formaldehyde, and amines, is a good molecule to apply since its ring opening always leads to *N,N'*-bis(2-hydroxybenzyl) alkylamines, namely benzoxazine dimers.<sup>27, 28</sup> Previously, it was demonstrated that strong inter- and intramolecular hydrogen bonds (N-H...O-H) of the dimers develop self-assemblies. By simply changing monoamine to diamines as shown in Scheme 1, a series of satisfied symmetrical molecules can be obtained with the phenol units for hydrogen bonds at both terminals and the variable alkyl chains in between for tuning the hydrophobicity.

<sup>a</sup> The Petroleum and Petrochemical College, Chulalongkorn University, Bangkok 10330, Thailand.

<sup>b</sup> Department of Future Industry-oriented Basic Science and Materials, Toyota Technological Institute, Tempaku, Nagoya 468-8511, Japan. E-mail: ktashiro@toyota-ti.ac.jp

<sup>c</sup> Center for Petroleum, Petrochemical, and Advance Materials, Chulalongkorn University, Bangkok 10330, Thailand. E-mail: csuwabun@chula.ac.th

† Electronic Supplementary Information (ESI) available: See DOI: 10.1039/x0xx00000x

## 1 Experimental Section

### 2 Materials

3 2,4-dimethylphenol, ethylenediamine, butamethylenediamine,  
4 hexamethylenediamine, octamethylenediamine, deuterated  
5 dimethylsulfoxide (DMSO- $d_6$ ), and deuterated chloroform  
6 ( $CDCl_3$ ) were purchased from Sigma-Aldrich. Formaldehyde  
7 solution (37%), 1,4-dioxane, 2-propanol, diethylether, and  
8 chloroform were obtained from Wako Pure Chemical Industries.  
9 Sodium hydroxide and sodium sulfate anhydrous were received  
10 from Fluka. All chemicals were used without further purification.

### 11 Synthesis of Compound C2, C4, C6, and C8.

12 All compounds were synthesized using the same synthetic  
13 procedure which modified from the literature.<sup>29</sup> In brief, 2,4-  
14 dimethylphenol (2 equiv) was reacted with paraformaldehyde (4.1  
15 equiv) and the corresponding diamine (1 equiv) in chloroform at  
16 70°C until a white solid was obtained. Then, the ring-opening  
17 reaction was carried out in the presence of chloroform 30% w/w  
18 by adding 2,4-dimethylphenol (2 equiv) and allowed stirring at  
19 120°C until a yellow viscous was obtained. The crude product was  
20 further purified by crystallization in a mixed solvent of chloroform  
21 and methanol (1:1, v/v). The white crystals were dried to yield the  
22 product.

23 *Characterization Data for 6,6',6'',6'''-(ethane-1,2-diylbis*  
24 *(azanetriyl))tetrakis(methylene)tetrakis(2,4-dimethylphenol)(C2).*  
25 Yield: 82%;  $^1H$  NMR (500 MHz, DMSO):  $\delta$  2.09 (12H, s), 2.14  
26 (12H, s), 2.33 (4H, t), 3.60 (8H, s), 6.71 (4H, s), 6.77 (4H, s), 9.47  
27 (4H, br). ESI-MS:  $m/z$  596.8.

28 *Characterization Data for 6,6',6'',6'''-(butane-1,4-diylbis*  
29 *(azanetriyl))tetrakis(methylene) tetrakis (2,4-dimethylphenol)*  
30 *(C4).* Yield: 87%;  $^1H$  NMR (500 MHz, DMSO):  $\delta$  1.41 (4H, m),  
31 2.09 (12H, s), 2.14 (12H, s), 2.32 (4H, t), 3.56 (8H, s), 6.70 (4H,  
32 s), 6.78 (4H, s), 9.47 (4H, br). ESI-MS:  $m/z$  624.85.

33 *Characterization Data for 6,6',6'',6'''-(hexane-1,6-diylbis*  
34 *(azanetriyl))tetrakis(methylene) tetrakis (2,4-dimethylphenol)*  
35 *(C6).* Yield: 92%;  $^1H$  NMR (500 MHz, DMSO):  $\delta$  1.04 (4H, m)  
36 1.43 (4H, m), 2.08 (12H, s), 2.13 (12H, s), 2.33 (4H, t), 3.57 (8H,  
37 s), 6.70 (4H, s), 6.77 (4H, s), 9.49 (4H, br). ESI-MS:  $m/z$  652.9.

38 *Characterization Data for 6,6',6'',6'''-(octane-1,8-diylbis*  
39 *(azanetriyl))tetrakis(methylene) tetrakis(2,4-dimethylphenol) (C8).*  
40 Yield: 90%;  $^1H$  NMR (500 MHz, DMSO):  $\delta$  1.06 (8H, m) 1.46  
41 (4H, m), 2.09 (12H, s), 2.14 (12H, s), 2.36 (4H, t), 3.59 (8H, s),  
42 6.71 (4H, s), 6.78 (4H, s), 9.46 (4H, br). ESI-MS:  $m/z$  680.9.

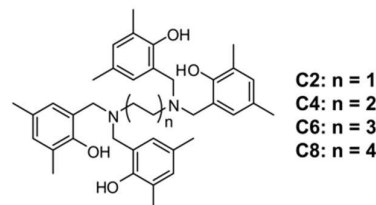
### 43 Characterizations.

44  $^1H$  NMR spectra were recorded on a Bruker Ultrashield Plus NMR  
45 spectrometer operating at Larmor frequencies of 500.13 MHz. For  
46 spin-lattice relaxation time ( $T_1$ ) measurements,  $T_1$  value was  
47 evaluated from inversion recovery ( $\pi-\tau-\pi/2$ ) measurements at a  
48 controlled temperature. Mass spectroscopy was analyzed by a  
49 Bruker micrOTOF II electrospray ionization mass spectrometer  
50 (ESI-MS). Single crystal structure analysis was carried out by a  
51 Rigaku R-axis Varimax X-ray diffractometer with graphite  
52 monochromated MoK $\alpha$  radiation at 296 K. The structures were  
53 determined by the direct method (SIR92) and refined by full-

54 matrix least-squares on  $F^2$  with a RAPID AUTO program. All  
55 non-hydrogen atoms were refined with anisotropic displacement  
56 parameters as well as the fractional coordinates. The single  
57 crystals were obtained from recrystallization in DMSO. The  
58 compounds were dissolved in DMSO as defined concentration, a  
59 drop of which was dispersed on an amorphous carbon film  
60 supported by a Cu grid for transmission electron microscopy. A  
61 Hitachi H-7650 transmission electron microscope (TEM)  
62 operating at an accelerating voltage of 100 kV and equipped with a  
63 double tilt holder was used for imaging and electron diffraction.

## 64 Results and Discussion

65 A series of diaminetetraphenol derivatives, hereinafter,  
66 diamine-based benzoxazine dimers, with methylene  
67 segmental length  $-(CH_2)_m-$  with  $m = 2, 4, 6$ , and 8 were  
68 synthesized as shown in Scheme 1.  
69



70  
71 **Scheme 1.** Diamine-based benzoxazine dimers with different alkyl chain  
72 lengths.

73 The molecular assemblies of **C2**, **C4**, **C6**, and **C8** via  
74 hydrogen bond in the solution state were examined by  
75 evaluating spin-lattice relaxation ( $T_1$  relaxation) using  $^1H$   
76 NMR in DMSO- $d_6$  under different concentrations and  
77 temperatures.  $T_1$  relaxation is a parameter representing the  
78 energy exchange between individual nuclear spins and the  
79 surrounding liquid or solid lattice.<sup>30, 31</sup> Basically, when the  
80 molecules form an interaction with each other, the interaction  
81 obstructs the degree of freedom of the molecules resulting in  
82 the short  $T_1$  relaxation time. Therefore, the differences in  $T_1$   
83 reflect the molecular self-assembly under the specific  
84 interaction, especially the hydrogen bond. To investigate this  
85 in detail, the hydroxyl protons at about 9.57 ppm were  
86 focused (Figure 1 (a)), and it was found that the  $T_1$  value at  
87 this position significantly changes with the concentration. For  
88 example, in the case of **C2**, the value gradually decreased as  
89 the concentration increased, as it did for those of **C4** and **C6**,  
90 but more rapidly. This suggests that **C2**, **C4** and **C6** might be  
91 in a tight environment where hydroxyl group play the  
92 important role in forming intermolecular hydrogen network  
93 resulting in the self-assembly. It should be noted that  
94 hydrogen bond network of **C2** might be initiated in the  
95 different way with **C4** and **C6**, which shown in slightly  
96 decrease of  $T_1$  value comparing to **C4** and **C6**. In the case of  
97 **C8**, the  $T_1$  value did not show any significant change as the  
98 concentration increased. It might be due to **C8** has no any  
99 intermolecular hydrogen bonding to create the self-assembly.

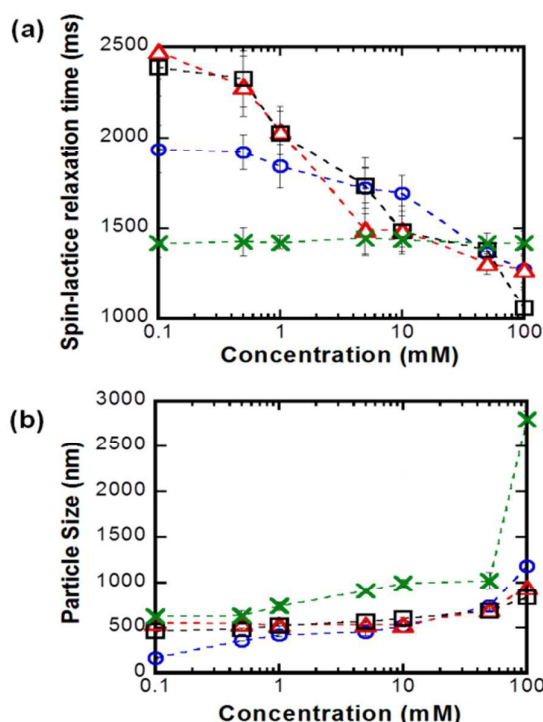


**Fig. 1** (a) Spin-lattice relaxation time ( $T_1$ ) and (b) self-assembly particle size of **C2** (○), **C4** (Δ), **C6** (□), and **C8** (×) under varying concentrations.

The size of self-assembly in solution was measured by dynamic light scattering (DLS) by using DMSO as solvent. Figure 1(b) shows that the size of **C2** is around 165 nm at the low concentration (1 mM) and gradually increases to 500 nm and to 1 μm when the concentrations reached 10 mM and 100 mM, respectively. Whereas **C4** and **C6** show the similar sizes of about 500 nm at the low concentration and become as large as 900 nm when the concentration is as high as 100 mM. In the case of **C8**, the particle size increases from 600 nm at 0.1 mM to 1 μm at 50 mM. Notably, when the concentration was up to 100 mM, the size rapidly increased to as high as 2.8 μm. This extremely increased in particle size of **C8** indicates that **C8** may not form the supramolecular assembly.

In fact, the  $T_1$  values obtained from NMR and the particle sizes obtained from DLS, reflected the self-assembly phenomenon in solution state. This leads to the question that how the self-assembly forms in the solid-state. Thus, all derivatives were dissolved in DMSO with various concentrations before drying to observe the developed morphologies by TEM. In fact, chloroform and DMSO were good solvent to dissolve all compounds as high as 100 mM. However, in order to study the morphologies in the same condition as single crystal, DMSO was applied.

As seen in Figure 2, the morphologies are found to be significantly fine-tuned by the concentrations. For example, **C2** changes from the donut-like at 0.001 mM to the round shape at 1.0 mM and 100 mM. Both **C4** and **C6** express the fiber morphology but with different branching. It is clear that **C8** shows irregular particles, especially in the low concentration (Figure 2 (j)).

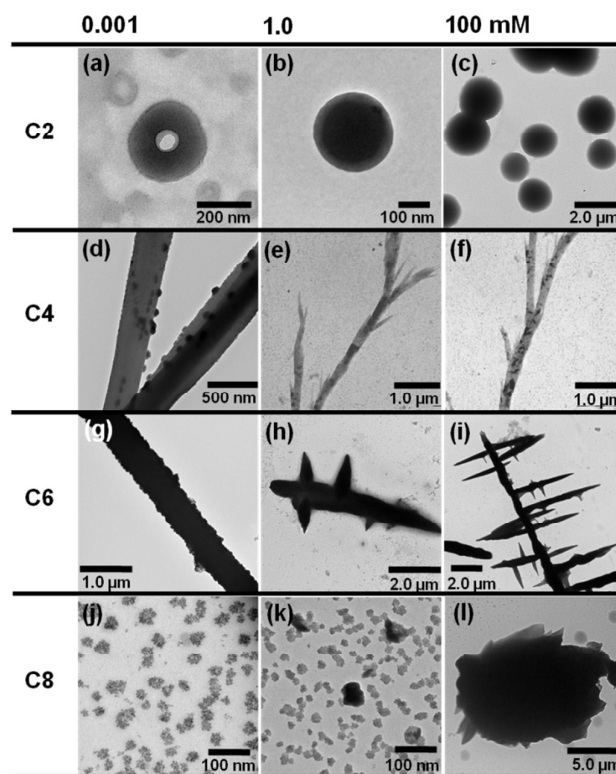


**Fig. 2** TEM micrographs of **C2**, **C4**, **C6**, and **C8** obtained from DMSO solutions with concentration of 0.001 mM for (a), (d), (g), and (f), concentration of 1.0 mM for (b), (e), (h), and (k), and concentration of 100 mM for (c), (f), (i), and (l).

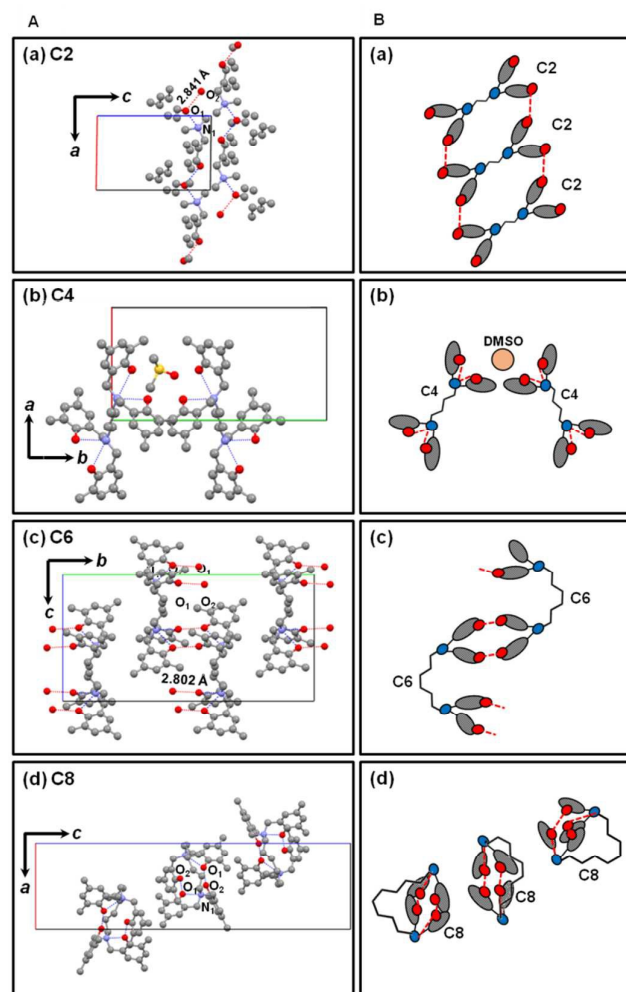
As **C2**, **C4**, **C6**, and **C8** exhibit different morphologies; this implies how the alkyl chains - in other words, the methylene bridges - play a key role in the hydrogen bond formation. At this point, it could be pointed out that the molecular assembly formations were governed by the factors of the hydrogen bond pattern and alkyl bridge length, or hydrophobicity. To clarify this point, the crystal lattices were investigated using X-ray single crystal structure analyses. Here, the single crystals were grown slowly from the DMSO solutions, since chloroform didn't give the good crystals for us. As shown in Figure 3A (a), the **C2** crystal is in the triclinic system ( $P\bar{1}$ ) with not only the intramolecular hydrogen bonds between N1 and O1 atoms, but also the intermolecular hydrogen bonds between O1 and O2 atoms with the distance of 2.84 Å. The molecules are in the extending, or stretching, structure. Figure 3B (a) illustrates the packing structures of **C2** by emphasizing the hydrogen bonds and tilting of the molecules. The **C4** is monoclinic ( $P2_1/c$ ) with DMSO molecules entrapped in the unit cell (Figure 3A (b)). In this case, only the intramolecular hydrogen bond is observed, implying that the **C4** assembly is stabilized by the hydrogen bonds with the solvent molecules rather than by the intermolecular hydrogen bonds. The **C6** molecules are bridged together by the solvent molecules. For **C6**, the crystal structure is monoclinic ( $C2/c$ ) with the intermolecular hydrogen bonds between O1 and O2 atoms along the  $c$ -axis direction (Figure 3A (c)). It is important to note that the crystal structure of **C6** in the connected molecular packing implies the possibility of a supramolecular polymer. For **C8**, the crystal structure is tetragonal ( $P4_12_12$ ), where no intermolecular hydrogen bond exists in the crystal



1 lattice. Only the intramolecular hydrogen bond is detected  
2 between N1 and O2 with the distance of 2.68 Å and between  
3 O1 and O2 atoms with 2.83 Å distance (Figure 3A (d)). In  
4 other words, the molecules are in dimer-rings. From this  
5 analysis, it is clear that the systematic variation of the alkyl  
6 chain length affects the differences of hydrogen bond patterns  
7 and the packing mode for the unique morphologies formation.

8 Furthermore, in order to clarify the development of the  
9 molecular arrangement and hydrogen bond patterns in the  
10 assembly, the electron diffraction patterns obtained from the  
11 TEM measurements were compared with the X-ray  
12 diffraction patterns.

13



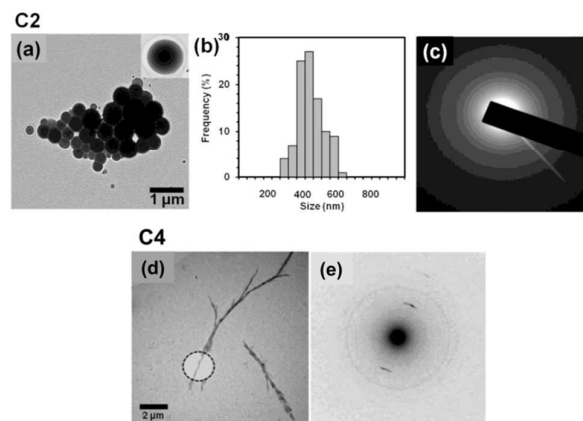
14  
15  
16  
17 **Fig. 3** (A) Crystal structures and (B) schematic illustrations of the intra- and  
18 intermolecular hydrogen bonds and their types of packing structures: (a) **C2**,  
19 (the extended packing), (b) **C4** (the solvent bridged packing), (c) **C6** (the  
20 connected molecular packing), and (d) **C8** (the dimer ring packing).

21

22 The TEM micrograph of **C2** shows the spherical  
23 morphology (Figure 4 (a)) with an average diameter of 250-  
24 500 nm (Figure 4 (b)). In the case of **C4**, the morphology  
25 shows the bunch of fibers with branches (Figure 4 (d)). The  
26 electron diffraction pattern shows the crystalline unit cells in  
27 the oriented fibers (Figure 4 (e)). The fibers are as long as  
28 tens of micrometers with the diameter ~200 nm. The  
29 morphology of **C8** is quite different from those of the others  
30 as it shows a random particulate shape. It is important to note

31 that no clear spots were detected in the electron diffraction  
32 patterns for **C2** (Figure 4 (c)) and **C8**, implying that the  
33 molecular assemblies of both cases might not be in a highly  
34 ordered structure. Considering other results, especially from  
35 the X-ray single crystal analysis (Figures 2 (j), (k), (l) and  
36 Figure 3(d)), it is clear that the packing structure might be  
37 satisfied with only intramolecular hydrogen bonds until no  
38 molecular assembly can be formed.

39

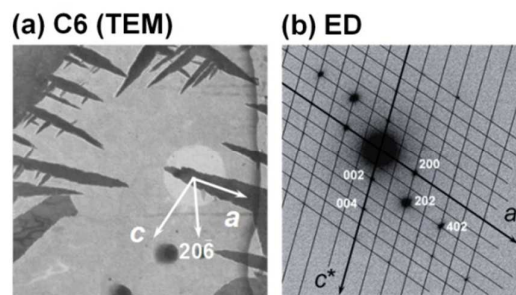


40  
41 **Fig. 4** TEM micrographs of **C2**: (a) morphology, (b) size distribution, and (c)  
42 electron diffraction pattern, and of **C4**: (d) morphology, and (e) electron  
43 diffraction pattern.

44

45 As **C6** shows the dendritic needles (Figure 5 (a)), with a  
46 clear electron diffraction pattern (Figure 5 (b)), the detailed  
47 analysis was carried out. It should be pointed out that the  
48 diffraction pattern is relevant to the crystal structure identified  
49 by X-ray single crystal analysis; therefore, it is expected that  
50 the superimposition between two images (figure 5 (a) and (b))  
51 might allow identification of the axis direction and growth of  
52 molecular assemblies. On the basis of the crystal structure  
53 information obtained from the X-ray structure analysis  
54 (Figure 3(c)), the electron diffraction pattern of **C6** with the  
55 orientation of crystallographic axes can be determined (Figure  
56 5 (b)). The growing direction of the long needle is found to  
57 be parallel to the *a*-axis. The branches are stretching from the  
58 main needle in the [206] direction to grow along the *a*-axial  
59 direction individually (Figure 5 (a)).

60



61  
62 **Fig. 5** (a) TEM micrograph of **C6** with the crystal axes. The side branches are  
63 created along the [206] direction of the main needle, and (b) electron  
64 diffraction (ED) diagram taken from the main needle (the bright circle shown  
65 in (a)) and the indexing.

66

Although several cases of supramolecular structures and their unique morphologies were reported, the molecular alignment from single molecules to self-assembly until the definite morphologies developed is still the point to be clarified. Here, an attempt to illustrate the morphologies from the molecular level was carried out. Figure 6 is the scheme showing the growth of the needle crystallites of **C6** along the *a*-axial direction. At that time, the **C6** molecules are stacked in the *bc* plane using intermolecular hydrogen bonds, and these stacked layers are attached onto the end of the needle crystallite in the growing process. It is expected that a similar situation might occur in the case of **C4** crystals.

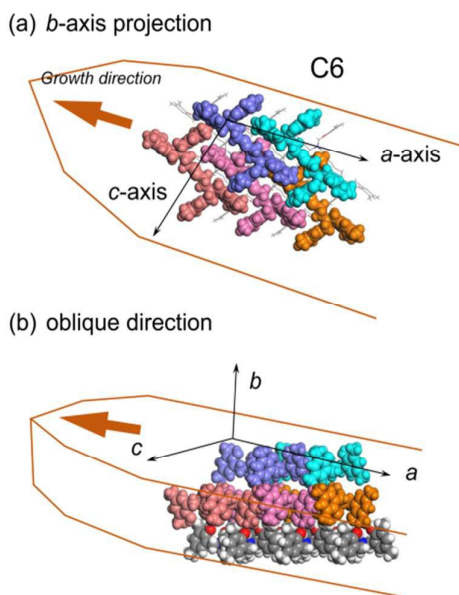


**Fig. 6** Schematic representation of needle growth of **C6** based on the superimposition of the needle axis and crystallographic axis: (a) *b*-axis projection and (b) the view from the oblique direction. The stacked molecular layers are attached step by step on the surface of the *bc* plane or along the *a*-axis.

Taking the effect of concentration as shown in Figure 2 back to our consideration, it is speculated that **C2**–**C6** might form the nanostructures based on the hydrogen bond networks which were under the effect of alkyl chains. In other words, the hydrophobic alkyl chains played an important role to control the packing structure on top of the intermolecular hydrogen bonds. Therefore, when the concentration increased, the packing structure might be developed differently as a consequence of hydrophobic interaction. In this way, for example **C2** either in the low concentration or in the high concentration, it shares the common mechanism as mentioned above, the sphere at high concentration might be a consequence of tightly packed assemblies under the two methylene unit of alkyl chain. The common mechanism, but depending on the alkyl chain length, can also be seen in the cases of **C4**, and **C6** (Figure 2) which the branching and dendritic were developed at the high concentration.

It is known that self-assembly and its definite morphology can be tuned depending on the environments such as concentration<sup>22, 32</sup>, temperature<sup>33</sup>, pH<sup>34</sup>, drying methods<sup>12</sup>, and types of solvent<sup>35</sup>. As chloroform is also a good solvent of these derivatives, their morphologies were observed to see how the environment affects molecular assemblies. Figure 7 shows the morphologies of all derivatives obtained by 1.0 mM concentration. It is clear that **C2** performs its spherical

shape, whereas **C4** and **C6** show the fine needle shape. The results are similar to those obtained from DMSO.

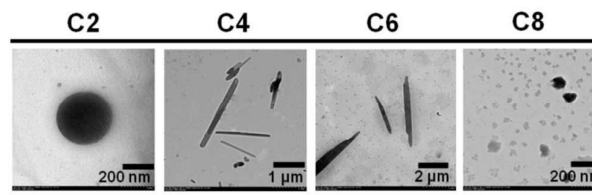


**Fig. 7** TEM micrographs of **C2**, **C4**, **C6**, and **C8** molecular assemblies obtained from the CHCl<sub>3</sub> solutions at the concentration of 1.0 mM.

## Conclusions

Diamine-based benzoxazine dimers represents a good example of the molecular assembly that can be fine-tuned by simply varying the alkyl building blocks of the molecules. The single crystal structure analysis as well as the superimposition between X-ray single crystal structure and electron diffraction pattern insisted that the molecular assemblies were basically formed by the hydrogen bonds, while they were further governed by the hydrophobic segment to tilt the packing structures. Therefore, the variation of the alkyl chain units and the concentration brought a significant change of the nano-scale structures to be donuts, spheres, needles, and dendrites. In addition, the solvent, such as DMSO, might also contribute to the supramolecular network. The present work, for the first time, shows the molecular assemblies under the hydrogen bond networks which were, in fact, primarily controlled by the hydrophobicity of the molecules.

## Acknowledgements

The authors would like to express their gratitude to the Thailand Research Fund (the Royal Golden Jubilee Ph.D. Scholarship, Grant No. PHD/0067/2553), Basic Research Grant (BRG-5380010), the 90th Anniversary of Chulalongkorn University Fund (Ratchadaphiseksomphot Endowment Fund), and the Japan Student Services Organization (JASSO) for financial support. The authors acknowledge Hitachi High Technology, Japan for TEM measurement. One of the authors (P. T.) would like to thank Dr. Taiyo Yoshioka for TEM-electron diffraction measurement.

## Notes and References

- 1 A. Barnard, P. Posocco, S. Pricl, M. Calderon, R. Haag, M. E. Hwang, V. W. T. Shum, D. W. Pack and D. K. Smith, *Journal of the American Chemical Society*, 2011, 133, 20288–20300.
- 2 P. Rajamalli and E. Prasad, *Langmuir*, 2013, 29, 1609–1617.
- 3 K. Ariga, T. Nakanishi and J. P. Hill, *Current Opinion in Colloid & Interface Science*, 2007, 12, 106–120.
- 4 Y. B. Zheng, B. K. Pathem, J. N. Hohman, J. C. Thomas, M. Kim and P. S. Weiss, *Advanced Materials*, 2013, 25, 302–312.
- 5 Y. Yang, W. Feng, J. Hu, S. Zou, R. Gao, K. Yamato, M. Kline, Z. Cai, Y. Gao, Y. Wang, Y. Li, Y. Yang, L. Yuan, X. C. Zeng and B. Gong, *Journal of the American Chemical Society*, 2011, 133, 18590–18593.

- 1 6 S. Lee, S. Oh, J. Lee, Y. Malpani, Y.-S. Jung, B. Kang, J.
- 2 Y. Lee, K. Ozasa, T. Isoshima, S. Y. Lee, M. Hara, D.
- 3 Hashizume and J.-M. Kim, *Langmuir*, 2013, 29, 5869-5877.
- 4 7 P. Bombicz, T. Gruber, C. Fischer, E. Weber and A.
- 5 Kalman, *CrystEngComm*, 2014, 16, 3646-3654.
- 6 8 J. He, X. Huang, Y.-C. Li, Y. Liu, T. Babu, M. A. Aronova,
- 7 S. Wang, Z. Lu, X. Chen and Z. Nie, *Journal of the*
- 8 *American Chemical Society*, 2013, 135, 7974-7984.
- 9 9 M. Antonietti and S. Förster, *Advanced Materials*, 2003, 15,
- 10 1323-1333.
- 11 10 S. Chiruvolu, S. Walker, J. Israelachvili, F. J. Schmitt, D.
- 12 Leckband and J. A. Zasadzinski, *Science (New York,*
- 13 *N.Y.)*, 1994, 264, 1753-1756.
- 14 11 T. Sun, Q. Guo, C. Zhang, J. Hao, P. Xing, J. Su, S. Li, A.
- 15 Hao and G. Liu, *Langmuir*, 2012, 28, 8625-8636.
- 16 12 G. Sun and C.-C. Chu, *ACS Nano*, 2009, 3, 1176-1182.
- 17 13 A. Aggeli, I. A. Nyrkova, M. Bell, R. Harding, L. Carrick,
- 18 T. C. B. McLeish, A. N. Semenov and N. Boden,
- 19 *Proceedings of the National Academy of Sciences of the*
- 20 *United States of America*, 2001, 98, 11857-11862.
- 21 14 C. Li, M. Numata, A.-H. Bae, K. Sakurai and S. Shinkai,
- 22 *Journal of the American Chemical Society*, 2005, 127,
- 23 4548-4549.
- 24 15 J. Puigmarti-Luis, A. Minoia, S. Lei, V. Geskin, B. Li, R.
- 25 Lazzaroni, S. De Feyter and D. B. Amabilino, *Chemical*
- 26 *Science*, 2011, 2, 1945-1951.
- 27 16 S. V. Rosokha, C. L. Stern and J. T. Ritzert,
- 28 *CrystEngComm*, 2013, 15, 10638-10647.
- 29 17 Y. Sun, C. He, K. Sun, Y. Li, H. Dong, Z. Wang and Z. Li,
- 30 *Langmuir*, 2011, 27, 11364-11371.
- 31 18 S. Ahmed, J. H. Mondal, N. Behera and D. Das, *Langmuir*,
- 32 2013, 29, 14274-14283.
- 33 19 S.-C. Lin, T.-F. Lin, R.-M. Ho, C.-Y. Chang and C.-S. Hsu,
- 34 *Advanced Functional Materials*, 2008, 18, 3386-3394.
- 35 20 B. Donnio, S. Buathong, I. Bury and D. Guillon, *Chemical*
- 36 *Society Reviews*, 2007, 36, 1495-1513.
- 37 21 A. Vidyasagar, K. Handore and K. M. Sureshan,
- 38 *Angewandte Chemie International Edition*, 2011, 50, 8021-
- 39 8024.
- 40 22 L. C. Palmer and S. I. Stupp, *Accounts of Chemical*
- 41 *Research*, 2008, 41, 1674-1684.
- 42 23 X. Zhang and C. Wang, *Chemical Society Reviews*, 2011,
- 43 40, 94-101.
- 44 24 L. Xu, X. Miao, B. Zha, K. Miao and W. Deng, *J. Phys.*
- 45 *Chem. C*, 2013, 117, 12707-12714.
- 46 25 D. S. Janni and M. K. Manheri, *Langmuir*, 2013, 29, 15182-
- 47 15190.
- 48 26 T. J. Moyer, H. Cui and S. I. Stupp, *J. Phys. Chem. B*, 2012,
- 49 117, 4604-4610.
- 50 27 A. Laobuthee, S. Chirachanchai, H. Ishida and K. Tashiro,
- 51 *J. Am. Chem. Soc.*, 2001, 123, 9947-9955.
- 52 28 S. Phongtamrug, K. Tashiro, M. Miyata and S.
- 53 Chirachanchai, *J. Phys. Chem. B*, 2006, 110, 21365-21370.
- 54 29 C. S. Higham, D. P. Dowling, J. L. Shaw, A. Cetin, C. J.
- 55 Ziegler and J. R. Farrell, *Tetrahedron Letters*, 2006, 47,
- 56 4419-4423.
- 57 30 L. Yuan, H. Zeng, K. Yamato, A. R. Sanford, W. Feng, H.
- 58 S. Atreya, D. K. Sukumaran, T. Szyperksi and B. Gong,
- 59 *Journal of the American Chemical Society*, 2004, 126,
- 60 16528-16537.
- 61 31 L. Brunsveld, H. Zhang, M. Glasbeek, J. A. J. M.
- 62 Vekemans and E. W. Meijer, *Journal of the American*
- 63 *Chemical Society*, 2000, 122, 6175-6182.
- 64 32 M. M. J. Smulders, M. M. L. Nieuwenhuizen, M.
- 65 Grossman, I. A. W. Pilot, C. C. Lee, T. F. A. de Greef, A.
- 66 P. H. J. Schenning, A. R. A. Palmans and E. W. Meijer,
- 67 *Macromolecules*, 2011, 44, 6581-6587.
- 68 33 C. Marie, F. Silly, L. Tortech, K. Müllen and D. Fichou,
- 69 *ACS Nano*, 2010, 4, 1288-1292.
- 70 34 M. T. Fenske, W. Meyer-Zaika, H.-G. Korth, H. Vieker, A.
- 71 Turchanin and C. Schmuck, *Journal of the American*
- 72 *Chemical Society*, 2013, 135, 8342-8349.
- 73 35 A. K. Boal, F. Ilhan, J. E. DeRouchey, T. Thurn-Albrecht,
- 74 T. P. Russell and V. M. Rotello, *Nature*, 2000, 404, 746-
- 75 748.
- 76

